IAEA
INTERNATIONAL ATOMIC ENERGY AGENCY

20th IAEA Fusion Energy Conference

Vilamoura, Portugal, 1-6 November 2004

IAEA-CN-116 / EX / 2-6

Integrated Exhaust Scenarios with Actively Controlled ELMs

P.T. Lang[1], A. Kallenbach[1], J. Bucalossi[2], G.D. Conway[1], A. Degeling[3], R. Dux[1], T. Eich[1], L. Fattorini[4], O. Gruber[1], S. Günter[1], A. Herrmann[1], L.D. Horton[1], S. Kalvin[5], G. Kocsis[5], J. Lister[3], M.E. Manso[4], M. Maraschek[1], Y. Martin[3], P.J. McCarthy[6], V. Mertens[1], R. Neu[1], J. Neuhauser[1], I. Nunes[4], T. Pütterich[1], W. Schneider[1], A.C.C. Sips[1], W. Suttrop[1], W. Treutterer[1], H. Zohm[1], and the ASDEX Upgrade Team

[1]Max-Planck-Institut für Plasmaphysik, EURATOM Association,
Boltzmannstr. 2, D-85748 Garching, Germany
[2] CEA Cadarache, 13108 St Paul-Lez-Durance Cedex, France
[3] CRPP-EPFL, Association EURATOM-Confédération Suisse, 1015 Lausanne, Switzerland
[4] Centro de Fusão Nuclear, Associacão EURATOM/IST,
Instituto Superior Técnico, 1049-001 Lisboa, Portugal
[5] KFKI-RMKI, EURATOM Association, P.O. Box 49, H-1525 Budapest-114, Hungary
[6] Department of Physics, University College Cork,
Association EURATOM-DCU, Cork, Ireland

Integrated Exhaust Scenarios with Actively Controlled ELMs

P.T. Lang[1], A. Kallenbach[1], J. Bucalossi[2], G.D. Conway[1], A. Degeling[3], R. Dux[1], T. Eich[1], L. Fattorini[4], O. Gruber[1], S. Günter[1], A. Herrmann[1], L.D. Horton[1], S. Kalvin[5], G. Kocsis[5], J. Lister[3], M.E. Manso[4], M. Maraschek[1], Y. Martin[3], P.J. McCarthy[6], V. Mertens[1], R. Neu[1], J. Neuhauser[1], I. Nunes[4], T. Pütterich[1], W. Schneider[1], A.C.C. Sips[1], W. Suttrop[1], W. Treutterer[1], H. Zohm[1], and the ASDEX Upgrade Team

[1]Max-Planck-Institut für Plasmaphysik, EURATOM Association,
Boltzmannstr. 2, D-85748 Garching, Germany
[2] CEA Cadarache, 13108 St Paul-Lez-Durance Cedex, France
[3] CRPP-EPFL, Association EURATOM-Confédération Suisse, 1015 Lausanne, Switzerland
[4] Centro de Fusão Nuclear, Associacão EURATOM/IST,
Instituto Superior Técnico, 1049-001 Lisboa, Portugal
[5] KFKI-RMKI, EURATOM Association, P.O. Box 49, H-1525 Budapest-114, Hungary
[6] Department of Physics, University College Cork,
Association EURATOM-DCU, Cork, Ireland
e-mail: peter.lang@ipp.mpg.de

Abstract An integrated high performance scenario based on simultaneous feedback control of the averaged divertor neutral particle and power flux has been established at ASDEX Upgrade. This approach is fully compatible with the present tungsten wall coating covering about 65 % of the plasma facing components and intended for application in the envisaged full-tungsten experiment. In our experiments, particle exhaust and divertor temperature derived from thermoelectric currents were tuned by acting on gas puff and argon injection rates. The ELM frequency is controlled by repetitive injection of small cryogenic deuterium pellets to avoid radiative instabilities occurring at low f_{ELM} and high radiated power and to control the ELM energy. No confinement loss is observed in this radiative type-I ELMy scenario with relatively flat density profiles. In contrast, similar type-III ELM scenarios achieved in hydrogen shows a relative confinement loss of 20 % as compared to the type-I phase. In parallel to pellets, alternative ELM trigger techniques like fast vertical plasma oscillations were developed and investigated as well. A particular experimental challenge for AUG conditions is to obtain a high pace making frequency.

1. Introduction

Active control of power and particle exhaust will be a necessary ingredient for future reactor-grade plasma scenarios. In parallel to suitable boundary conditions for the desired plasma core conditions, there are three requirements related to exhaust: The averaged power load has to be compliant with the divertor cooling system, which results in maximum power flux densities around 5-10 MW/m^2. The ELM energy has to be limited to avoid transient overheating of the plasma facing surface which would lead to material ablation and a shortening of the target lifetime [1]. The tool to control the ELM energy is to increase the ELM frequency above its natural value ('ELM pace making'), taking advantage of the empirical finding that the ELM power is reduced with frequency for triggered as well as for the intrinsic ELMs [2]. Finally, particle exhaust must be adjusted according to fuelling requirements, capacity of the tritium extraction plant and the necessary helium removal rate.

Another boundary condition will be imposed by plasma purity requirements. ITER in its reactor-like operation phase is likely to have, like a fusion reactor, full high-Z walls, with tungsten being the present first choice material. The combination of sputtering, edge and core impurity transport which determines the central high-Z concentration may impose limits to the plasma parameters in front of the wall surfaces which are tighter than those imposed by the cooling system or lifetime considerations. This means that, in addition to the exhaust control as mentioned above, high-Z impurities have to be kept at sufficiently low concentrations. In

parallel, the removal of carbon results in the missing of the primary intrinsic radiator, which poses a higher demand on the divertor power dissipation. ASDEX Upgrade is currently being transformed into a full tungsten covered tokamak, with presently 65 % of the plasma facing components coated with tungsten. En route towards a full metal machine, the plasma temperature where the primary radiative losses take place shifts towards higher values, since no extrinsic radiator exists which has the peak of the radiative loss function as low as carbon. As a consequence, power dissipation is shifted closer to the core plasma, and the operational point for given heating and target power comes closer to the H-L threshold, which is determined by the power flux in the pedestal region. The latter effect makes ELM and impurity behavior more delicate and results in an additional need for ELM frequency control. Pronounced central density peaking, which was used in the past to compensate for pedestal pressure losses caused by radiative cooling [3] is no longer an option in ASDEX Upgrade since central accumulation of tungsten would occur.

The paper is organized as follows. After a description of the experimental setup in the ASDEX Upgrade tokamak, the control systems and related diagnostics are described which are used for the integrated exhaust control scenario (IEC). Chapter 3 introduces the exhaust scenario and discusses various aspects of impurity transport. A comparison of the type-I ELMy scenario in deuterium with a type-III ELMy one in a similar hydrogen plasma is given to demonstrate the performance loss to be taken into account operating with benign type-III ELMs. Chapter 4 reviews briefly the physics associated with ELM control and finally different experimental techniques for ELM pace making are compared.

2. Experimental Setup

The above mentioned exhaust requirements can only be met with a versatile, multi-parametric feedback system. Experiments were conducted at ASDEX Upgrade (torus radius $R_0 = 1.65$ m, minor plasma radius $a_0 = 0.5$ m, plasma volume $V_{Plasma} = 13\ m^3$), in this campaign equipped with the divertor DIV IIb and 25 m^2 tungsten coated tiles covering the major part of the inner heat shield, the upper divertor, the lower inner and outer divertor baffles, the upper passive stabilization loop and a protection limiter on the low field side [4]. Additional heating was a mix of NBI and ICRH, the latter with its resonance close to the magnetic axis for density peaking control [5]. Experiments were done in lower single null configuration with a plasma current $I_P = 1MA$, safety factor $q_{95} = 3.9$, toroidal magnetic field $B_t = 2.0T$, and elevated upper and lower triangularity of $\delta^u = 0.2$ and $\delta^l = 0.4$, respectively. Feedback parameters for exhaust control are the neutral divertor flux as measured by a pressure gauge and the divertor temperature as derived from thermoelectric currents measured by shunts [6]. Actuators are deuterium valves and an argon valve situated in the outer midplane. The pellet frequency is preset, injection is possible at frequencies $f_{pel} = \frac{250}{n}, n \geq 3$. Practically, frequencies between 40 and 63 Hz were used to ensure good injection reliability of each pellet. For the experiments on ELM triggering by fast vertical plasma oscillations the driving frequency was restricted to 30 Hz $< f_D <$ 90 Hz to avoid vessel resonance.

3. Integrated exhaust scenario

Figure 1 shows time traces of a discharge were the three major exhaust parameters inter-ELM power, ELM power and particle removal rate have been controlled simultaneously while maintaining an acceptable central tungsten concentration. The duration between ELMs is kept at a maximum value of 25 ms by 40 Hz pellet injection from 2.8 to 5.8s. For longer inter-ELM phases, the plasma is prone to a radiative instability under these conditions, which would lead to a short H-L transition [7]. As shown in Fig. 1 and observed in other experiments [8] [9], the type-I ELM frequency is reduced during radiative cooling due to the reduced power flow over

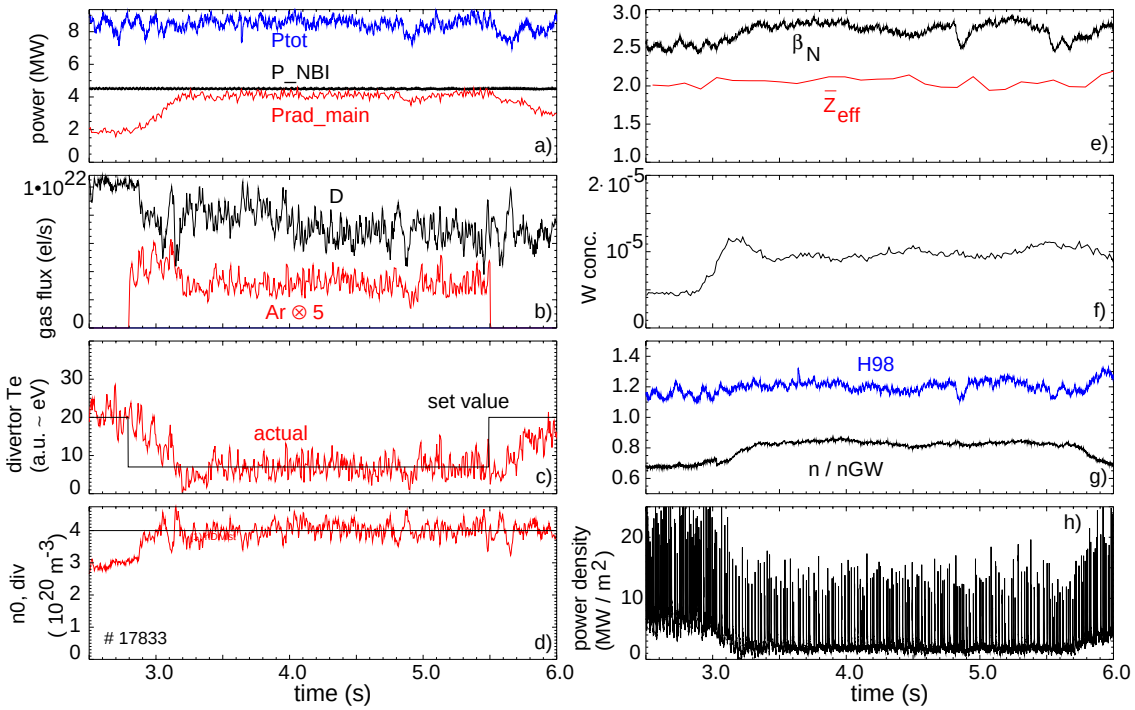

Figure 1: Discharge in the integrated exhaust controlled scenario. a) heating and main chamber radiated power. About 4 MW central ICRH was added to 4.5 MW NBI. b) gas valve fluxes, c) and d) set values and actual values of divertor temperature and neutral density, e) β_N and line-averaged Z_{eff} from bremsstrahlung, f) tungsten concentration around ρ_p= 0.7 from the W quasicontinuum, g) Greenwald fraction and H-factor according to the ITERH-98P(y, th) scaling and h) peak power density in the outer divertor from thermography.

the edge transport barrier (ETB) region. Additionally, the inter-ELM power flux at the outer target is drastically reduced, as shown in Fig. 2. Despite the frequency reduction and opposite to the standard relation, the ELM energy is reduced compared to the non-seeded phase. This can be explained either by the reduced power flux due to the radiation or by the increased collisionality in the pedestal region [10] at increased density and reduced temperature. In DIII-D it was shown that the conducted fraction of the ELM energy decreases with rising pedestal density, while the convection fraction remains about constant [11].

3.1. Impurity behavior The combination of high-Z wall and radiative cooling is an issue since sputtering by medium-Z ions is the dominant erosion mechanism [12]. Generally, the sputtering yield for a given impact energy rises with impinging ion mass. In contrast, the plasma seed impurity concentration decreases with mass in a realistic scenario, since the main plasma $\Delta P_{rad}/\Delta Z_{eff}$ rises with the impurity charge [13]. Multiplying the sputtering yield for an impurity ion with its concentration in the edge plasma gives an estimate of the resulting tungsten concentration, leaving out the effects of impurity transport. It turned out that for realistic plasma parameters the expected tungsten release is very similar for the elements C, Ne, Ar and Kr [7] [4]. Adding of seed impurities with a resulting increase of main plasma radiation is quite generally accompanied by a rise of the electron density in the core plasma, which is connected to an improvement of particle confinement. This is also observed in the type-I ELMy H-mode discharge shown in Fig. 1. Possible contributors to this effect are a deeper penetration of deuterium neutrals due to the edge cooling, a change of transport in the edge region and the reduction of ELM losses, which is evident from the clear reduction of the

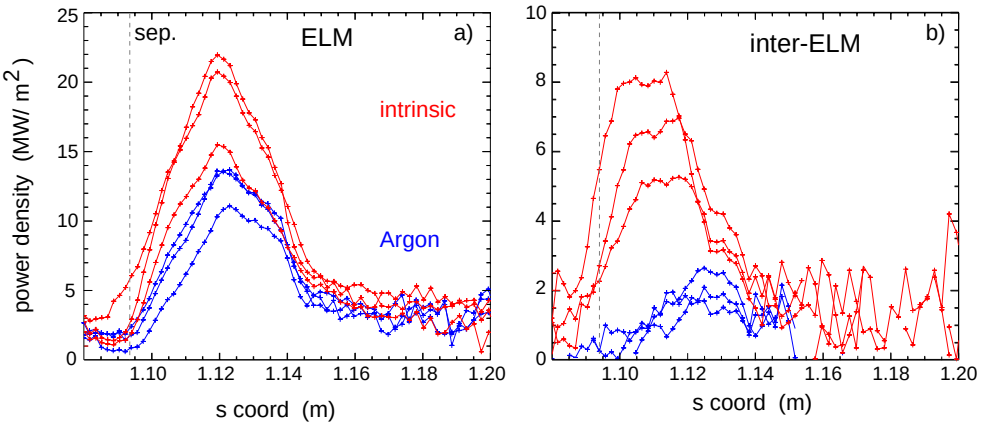

Figure 2: Outer target power load from IR thermography a) during the ELM peak and b) in between ELMs for the seeded (blue) and non-seeded (red) phases. 3 typical time points have been chosen to demonstrate variations between different ELMs and inter-ELM phases. Despite the reduction of the ELM frequency by Ar seeding from 108 to 60 Hz, the ELM power is reduced.

ELM frequency.
The experimental observations for discharges similar to that shown in Fig. 1 are as following: The tungsten influx from a low field side limiter as measured by visible spectroscopy [14] remains about constant during the Ar seed phase, while the tungsten concentration rises moderately. The carbon and hydrogen main chamber fluxes decrease, while the power flow into the divertor is significantly reduced (by 2 MW in the case shown in Fig. 1). As a consequence, the divertor radiation measured by bolometry is reduced as well, in line with an earlier observation that the divertor radiation is mainly proportional to the power flux into the divertor [15]. Analysis of CII and CIII spectral lines indicates a reduced carbon sputtering in the divertor during the Ar seed phase, while Ar itself does not contribute significantly to divertor radiation due to the temperature dependence of its radiative loss function.
The increased electron density during the Ar seed phase is related to an improved particle confinement time, since the neutral deuterium divertor flux is feedback controlled to a constant value. This is also in line with the observation of a constant core carbon density despite reduced sources. In summary, the higher electron density in combination with the additional Ar source leads to Z_{eff} remaining constant during the seed phase.

3.2. Importance of ELM frequency control for radiative stability The type-I ELM frequency is a key parameter for the impurity density near the pedestal top in the plasma core, since a strong ion inward pinch in the ETB region is observed during the inter-ELM phase [16]. As a consequence, the tungsten concentration as measured by a grazing incidence spectrometer depends inversely on f_{ELM} as shown in the l.h.s of Fig. 3. This trend is observed between different discharges as well as for individual ones comparing Ar seeded and non-seeded phases. Type-I ELMy discharges with high radiation level inside the separatrix are prone to the development of a radiative instability, as shown in the r.h.s. of Fig. 3. The instability is assumed to be caused by the reduction of the type-I ELM frequency with decreasing power flux through the ETB [17]: In between ELMs, the plasma radiation rises strongly. The resulting reduced power flux through the ETB further delays the next ELM. Finally, the radiation rises to a level where a H-L back transition occurs. The divertor plasma detaches immediately, the effective T_{div} derived from thermo currents goes to zero and the feedback system reacts with a closure of the Ar valve. Stable H-mode operation is reached again after typically 0.2 s.

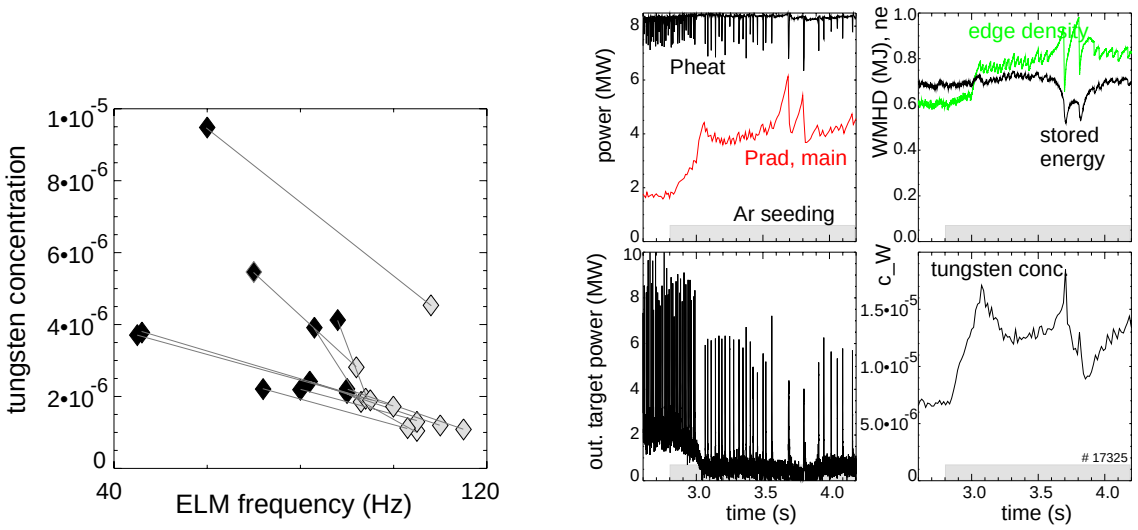

Figure 3: left: tungsten concentration vs. ELM frequency from the seeded (open symbols) and non-seeded phase (closed sym.) of discharges with Ar feedback. Straight lines connect different phases of the same discharge. right: time traces of a discharge with Ar cooling starting at 2.8 s without ELM pace making.

To avoid this unfavorable low frequency cycle, ELM pace making appears to be essential for stable radiative conditions close to the H-L boundary and also to keep the central tungsten concentration low.

3.3. Comparison of type-I vs. type-III ELMy regime The IEC discharges discussed above stay in the type-I ELMy regime, in contrast to completely detached (CDH-)mode discharges investigated earlier in Div-I. With the present Div-IIb, stable type-III phases could not be achieved by impurity seeding with high heating power and low-moderate deuterium puff. The reason is supposed to be related to the H-L and H-I - H-III power thresholds. To demonstrate the effect of the H-mode regime, the IEC scenario was applied to hydrogen discharges, where the increased H-mode power threshold allows easy access to the type-III regime.

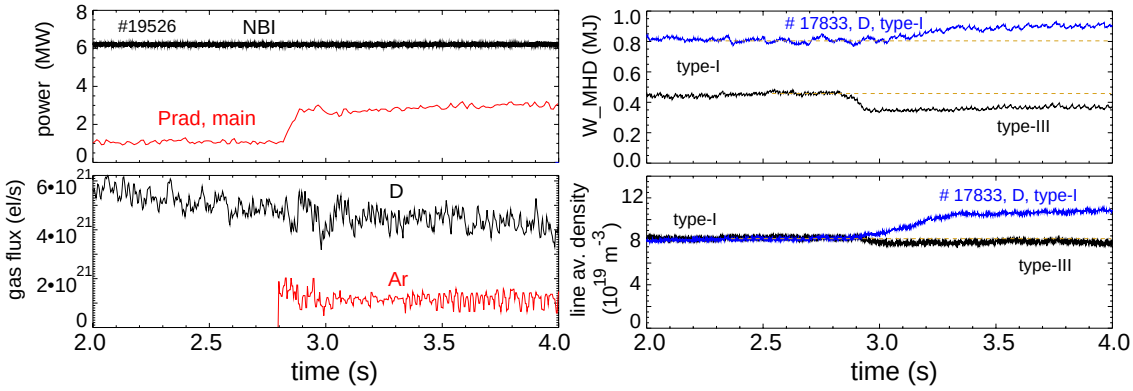

Figure 4: Radiative cooling scenario similar to that shown in Fig. 1 with hydrogen as working gas. During the cooling phase, the plasma enters the type-III ELMy regime. A clear drop in stored energy is seen and no change of the core density, in contrast to the type-I ELMy case in deuterium. No ELM pace making was applied here due to the high natural frequency.

Fig. 4 shows time traces of such a discharge which had a type-I $\rightarrow$ type-III transition after the start of the Ar injection. A clear drop of the energy content is observed which is caused by the

transition to type-III. The pronounced improvement of the particle confinement as seen in the corresponding type-I discharge shown in Fig. 1 is absent with type-III ELMs. Comparison of the relative reaction of energy and particle content on the Ar puff demonstrates the advantages of the type-I regime. However, control of the type-I ELM frequency is mandatory, and scalings need to be established to clarify how large this frequency must be to be compatible with the target material and what performance losses are related while this frequency is enforced.

4. ELM pace making

A search for methods aiming to destabilize MHD modes causing the ELM event was based on the present knowledge of the phenomena. Release of an ELM is thought to result from crossing the MHD stability boundary for coupled Peeling-Ballooning modes [18]. Perturbation of the related parameters, namely the current density and the pressure gradient in the ETB, seems therefore a plausible way to influence the ELM behavior. The most successful method for reliable and persistent ELM control employed so far is the injection of small cryogenic D pellets. Further techniques were investigated in order to find out possible alternative solution owing even more suitable features.

A suitable technique for ELM pace making has to fulfill three basic requirements:
the potential to impose external ELM control and enhancement of f_{ELM} beyond f^0_{ELM};
keeping a good plasma performance;
reduction of P_{ELM} at an enhanced f_{ELM} level.

4.1. Injection of small pellets D pellet injection can enhance and finally control the ELM frequency. This is shown in the left part of figure 5, displaying the ELM frequency in a set of discharges while performing a pellet frequency f_{Pel} scan. Initial pre-pellet phases had no auxiliary particle source ($\Gamma = 0$). During the post-pellet phase, a constant gas puff rate of $\Gamma_{Gas} = 8 \times 10^{20} D/s$ was applied to achieve parameters similar to those with pellet fuelling. Gas and pellet fuelling caused a density enhancement of about 10%. The discharges developed an intrinsic ELM frequency $f^0_{ELM} \approx 30$ Hz. Enhancement of f_{ELM} is already achieved for f_{Pel} still below f^0_{ELM} with a mixture of intrinsic and externally triggered ELMs during the control phases. Once $f_{Pel} \approx 1.5 \times f^0_{ELM}$ is reached, full control with $f_{Pel} = f_{ELM}$ is obtained. For the highest available pellet rate, a maximum enhancement of $f_{ELM} \approx 2.5 \times f^0_{ELM}$ is achieved. In order to clarify the extent and nature of resulting confinement losses, the impact of the frequency enhancement on plasma energy, as shown in the right part of figure 5, is inspected. There is a clear loss of plasma energy with raising f_{ELM}. However, this confinement reduction is quite modest, a least-square-fit to the data yield a correlation $W_{MHD} \sim f^{-0.16}_{ELM}$. This is significantly less severe as when acting via gas puffing. For the latter, a massive confinement degradation $W_{MHD} \sim f^{-0.6}_{ELM}$ is predicted from the empirical scaling derived for AUG and JET data [19]. Indeed, confinement reduction close to this scaling prediction was observed in a matching discharge where f^0_{ELM} was increased by a gas puff ramp. For this experiment, a gradually increasing gas puff was employed until at $\Gamma_{Gas} = 7 \times 10^{21} D/s$ matching of the main plasma parameters (indeed almost perfect matching even of density and temperature profiles) was realized with respect to the phase with $f_{ELM} = f_{Pel} = 83.3$ Hz. While plasmas became virtually identical in the matching phase, there was a striking difference in the ELM behavior with $f^0_{ELM} = 51$ Hz in the gas puffed discharge. The attempt for significant further increase of f_{ELM} by stronger gas puffing failed as the resulting massive confinement reduction eventually caused a loss of the type-I ELMy H-mode. This observation proves ELM control via pellets can extend the accessible operational space while inducing only a very modest impact on the confinement.

It was found that a reduction of the ELM induced plasma energy losses ΔW_{ELM} with f_{ELM} takes place for pellet triggered ELMs in exactly the same way as for intrinsic ELMs at JET and

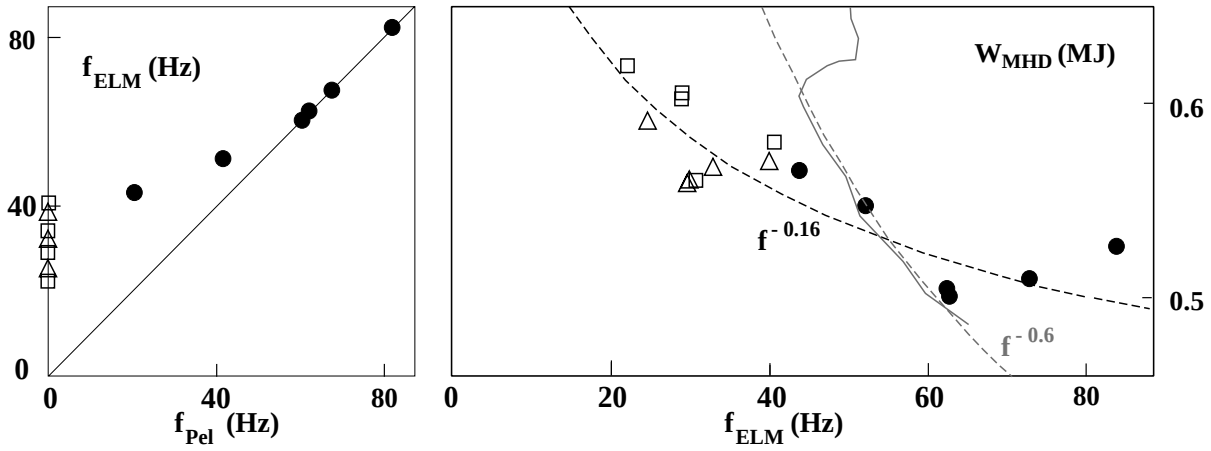

Figure 5: Demonstration of ELM pace making by pellets (left) and impact on confinement.(right) Data from pellet phases (dots) and reference phases without (squares) and with (triangles) gas puffing. Pellet f_{ELM} drive causes less confinement loss (black dashed) than raising by gas (gray solid, dash: scaling expectation).

ASDEX Upgrade [19]. Investigations of the ELM induced power load patterns on the divertor plates performed using infra-red thermography showed that there is no significant difference between pellet triggered and intrinsic ELM in magnitude and structure when comparing ELMs at the same f_{ELM} values. Furthermore, all the investigations performed so far found no differences in these ELMs dynamics once the ELM is released.

A caveat for the use of pellets for ELM triggering is their capability to trigger MHD modes. Investigations on the occurrence of NTM modes in JET and ASDEX Upgrade [20] showed pellets reaching the corresponding resonant flux surface triggered related modes as soon as they become virtually unstable. This deficiency may be overcome by the use of small pellets penetrating just to the pedestal top, which may be sufficient for ELM triggering as well as core fuelling support.

4.2. Magnetic triggering An alternative technique for ELM control is the magnetic triggering approach. Invented by TCV [21] it is based on a rapid vertical movement of the plasma column. The observed effect of locking the ELM time sequence with plasma oscillation is attributed to an edge current induction during the vertical movement in a spatially inhomogeneous single-null vacuum field configuration. We have adapted this method for type-I ELMy H-modes in the same discharges applied for the pellet approach. Shaking the plasma showed an immediate impact on the ELM behavior and once steady state conditions are reestablished locking of the ELMs to the motion with a driving frequency f_D could be achieved [22]. With this method, both an increase and a decrease of f_{ELM} were obtained. In our first proof-of-principle experiments an operational range of $\frac{f_D}{f^0_{ELM}} = 0.75 - 1.8$ was obtained. A relation $W \sim {f_{ELM}}^{-0.22\pm0.06}$ was observed similar to that found in the pellet case. Again, no significant difference was found when comparing intrinsic and triggered type-I ELMs. MHD mode activity still showed clear type-I features; for triggered ELMs, no precursor structures could be detected. As the ELMs fit again to scaling laws [19], this indicates ELM amelioration when driving up f_D.

In order to envisage further optimization of the magnetic triggering, a better understanding in the underlying physics is needed. It is still unknown why the general behavior at ASDEX Upgrade is inverted with respect to TCV. In our experiments, the ELM were triggered preferentially at a maximum downward velocity. The impact of the motion on the edge current seems to be the same in both experiments, ELM stabilization is achieved at ASDEX Upgrade whilst I_{edge} is

increased and vice versa, a behavior inverse to TCV's findings.

4.3. Injection of a supersonic gas jet An attempt has been made to replace cryogenic D pellets by fast D_2 gas. A Supersonic Pulsed Injector (SPI) [23] delivering a molecular deuterium gas jet was applied. Jets lasting about 2 ms were injected at a repetition rate of 2 Hz containing about $5 \times 10^{19} D_2$ through a Ø5 mm Laval nozzle throat at a speed of 2.2 km/s. Again, discharges applied for studies on pellets were used with a distance of 9 cm between nozzle and separatrix. No instant ELM trigger was initiated by the gas jet. The plasma reaction to SPI turned out to be similar to a standard gas puff, albeit with a better fuelling efficiency.

5. Discussion and conclusions

A tungsten-compatible plasma scenario with integrated exhaust control of ELM energy, inter-ELM power and particle removal rate has been established at ASDEX Upgrade. ELM triggering by small pellets was used to control and mitigate ELMs. As alternative technique, magnetic triggering by vertical oscillations of the plasma allowed to increase and decrease the ELM frequency, however, this technique has not been integrated into a routine scenario due to technical difficulties. The attempt to replace the pellets by supersonic pulsed gas injection failed to trigger ELMs instantaneously. This is supposed to be caused by insufficient penetration depth or localization of the perturbation.

As no significant differences between intrinsic and triggered ELMs could be detected, it seems their dynamics is independent from the trigger mechanism. The ELM frequency appears to be a very important parameter for the impurity concentration in the core plasma, since ELM particle losses counteract the strong inward transport of impurity ions in the inter-ELM phase. To establish parameter scans necessary for extrapolation to reactor conditions, a higher ELM trigger frequency is required. To allow for yet higher pellet rates beyond 100 Hz while keeping fuelling constraints negligible, a novel pellet blower gun injector is currently being developed.

References

[1] FEDERICI, F. et al., Plasma Phys. Controlled Fusion **45** (2003) 1523.
[2] LANG, P. T. et al., Nucl. Fusion **44** (2004) 665.
[3] KALLENBACH, A. et al., Plasma Phys. Controlled Fusion **38** (1996) 2097.
[4] NEU, R. et al., this conference .
[5] DUX, R. et al., this conference .
[6] KALLENBACH, A. et al., J. Nucl. Mater. **290-293** (2001) 639.
[7] KALLENBACH, A. et al., PSI 2004 Conf., Journal Nucl. Mat. in press (2004).
[8] HIGASHIJIMA, S. et al., J. Nucl. Mater. **313-316** (2003) 1123.
[9] MADDISON, G. et al., Nucl. Fusion **43** (2003) 49.
[10] LOARTE, A. et al., J. Nucl. Mater. **313-316** (2003) 962.
[11] LEONARD, A. et al., J. Nucl. Mater. **313-316** (2003) 768.
[12] THOMA, A. et al., Plasma Phys. Controlled Fusion **39** (1997) 1487.
[13] KALLENBACH, A. et al., Fusion Engineering and Design **36** (1997) 101.
[14] DUX, R. et al., PSI 2004 conf., Journal Nucl Mat. in press (2004).
[15] KALLENBACH, A. et al., Nucl. Fusion **39** (1999) 901.
[16] DUX, R., Fusion Science and Technology **44** (2003) 708.
[17] ZOHM, H., Plasma Phys. Controlled Fusion **38** (1996) 105.
[18] WILSON, H. R. et al., Nucl. Fusion **40** (2000) 713.
[19] HERRMANN, A., Plasma Phys. Controlled Fusion **44** (2002) 883.
[20] MARASCHEK, M. et al., EPS Conf. Abstracts 25 A (2001) 1801.
[21] DEGELING, A. W. et al., Plasma Phys. Controlled Fusion **45** (2003) 1637.
[22] LANG, P. T. et al., Plasma Phys. Controlled Fusion **46** (2004) L31.
[23] BUCALOSSI, J. et al., 19^{th} IAEA Conf., Lyon 2002, EX/P4-04 .